Characterization of Dynamic Interactions Between Cardiovascular Signals by Time-Frequency Coherence

Michele Orini*, Raquel Bailón, Luca T. Mainardi, Pablo Laguna, *Senior Member, IEEE*, and Patrick Flandrin, *Fellow, IEEE*

***Abstract*—An assessment of the dynamic interactions between cardiovascular signals can provide valuable information to improve the understanding of cardiovascular control. In this study, two methodologies for the characterization of time-frequency (TF) coherence between cardiovascular signals are described. The methodologies are based on the smoothed pseudo-Wigner–Ville distribution (SPWVD) and multitaper spectrogram (MTSP), and include the automatic assessment of the significance level of coherence estimates. The capability to correctly localize TF regions, where signals are locally coupled, is assessed using computer-generated data, and data from healthy volunteers. The SPWVD allows for the localization of these regions with higher accuracy (AC$>$96.9% for SNR$\geq$5 dB) than the MTSP (AC$>$84.4% for SNR$\geq$5 dB). In 14 healthy subjects, TF coherence analysis was used to describe the changes, which a tilt table test provokes in the cardiovascular control. Orthostatic stress provoked an increase in the coupling between R-R variability (RRV) and systolic arterial pressure variability; it did not provoke any significant changes in the coupling between RRV and respiration. In HF band, it decreased the strength of the coupling between RRV and pulse interval variability estimated from arterial pressure signal.**

***Index Terms*—Cardiovascular unteractions, multitaper spectragram, time-frequency coherence, Wigner-Ville distribution.**

Manuscript received May 2, 2011; revised August 27, 2011 and October 6, 2011; accepted October 6, 2011. Date of publication December 1, 2011; date of current version February 17, 2012. This work was supported in part by the Ministerio de Ciencia e Innovación, Spain, under Project TEC2010-21703-C03-02 and Project TRA2009-0127, by the Diputación General de Aragón, Spain, through Grupos Consolidados GTC ref:T30, by Instituto de Salud Carlos III, Spain, through CIBER CB06/01/0062, and by ARAID and Ibercaja under Project "Programa de apoyo a la I+D+i." *Asterisk indicates corresponding author*.

*M. Orini is with the Communications Technology Group (GTC), Aragón Institute of Engineering Research (I3A), IIS Aragón, University of Zaragoza, 50018 Zaragoza, Spain, and CIBER de Bioingeniería, Biomateriales y Nanomedicina (CIBER-BBN), Spain and also with the Department of Bioengineering, Politecnico di Milano, 20133 Milano, Italy (e-mail: morini@unizar.es).

R. Bailón and P. Laguna are with the Communications Technology Group (GTC), Aragón Institute of Engineering Research (I3A), IIS Aragón, University of Zaragoza, 50018 Zaragoza, Spain, and CIBER de Bioingeniería, Biomateriales y Nanomedicina (CIBER-BBN), Spain (e-mail: rbailon@unizar.es; laguna@unizar.es).

L. T. Mainardi is with the Department of Bioengineering, Politecnico di Milano, 20133 Milano, Italy (e-mail: luca.mainardi@biomed.polimi.it).

P. Flandrin is with the Physics Department (UMR 5672 CNRS), Ecole Normale Supérieure de Lyon, 69364 Lyon Cedex 07 France (e-mail: Patrick.Flandrin@ens-lyon.fr).

Color versions of one or more of the figures in this paper are available online at http://ieeexplore.ieee.org.

Digital Object Identifier 10.1109/TBME.2011.2171959

I. Introduction

SPECTRAL coherence measures the degree of correlation between the spectral components of two signals [1]. This measure, which requires signals to be stationary, is inappropriate for studying nonstationary processes. In the analysis of cardiovascular signals, the estimation of spectral coherence in the joint time-frequency (TF) domain has many potential fields of application. For example, the localization of TF regions in which two signals are coupled, can be applied to the time-varying estimation of baroreflex sensitivity [2]–[4], or in the assessment of the degree of similarity between different signals [5]. In recent years, different methods to estimate time-varying spectral coherence have been proposed. Most of them are based on parametric autoregressive modeling [6]–[8]. The performance of these methods is related to the goodness of fit with a predefined model, and in extremely nonstationary conditions they have been observed to perform less accurately than nonparametric methods [9]. Coherence estimators based on nonparametric methods have the advantage of not requiring any assumption on the TF structure of the signals, and are relatively easy to estimate. Among them, in biomedical applications, measures of time-scale coherence based on continuous wavelet transform (WT) have been recently proposed to study cardiovascular dynamics [4], [10] as well as neural connectivity [11], [12]. The TF resolution of the WT depends on frequency. This implies that in the same signal slower oscillations are localized with lower temporal resolution, while the faster ones are localized with lower spectral resolution. In the late 1990s, estimators of time-frequency coherence (TFC) based on multitaper spectrogram were proposed to study the coupling between neuronal signals [13] and atrial fibrillation [14]; but, to the extent of our knowledge, they have never been used in the analysis of cardiovascular variability.

In this paper, two methods of TFC analysis are described with the purpose of demonstrating their usefulness in the characterization of dynamic cardiovascular interactions. One is based on the smoothed pseudo-Wigner–Ville distribution (SPWVD), and the other one on the multitaper spectrogram (MTSP). These methods include the possibility of automatically localizing TF regions in which spectral coherence is statistically significant. The accuracy in the localization of these regions is assessed in a simulation study. To highlight the potential of the presented methods, TFC analysis is used to characterize the changes induced by the tilt table test [15] on the dynamic interactions between R-R variability (RRV) and systolic arterial pressure

variability (SAPV), RRV and respiration (RESP), and RRV and arterial pulse interval variability (PIV). The characterization of the interactions between the RRV-SAPV signals and RRV-RESP signals is relevant since it gives valuable information about the baroreflex and the respiratory sinus arrhythmia. The TFC between RRV-PIV signals is estimated to assess whether the PIV signal can be used as a surrogate for the RRV signal.

II. Methods

The spectral coherence function between two stationary zero-mean random processes $x(t)$ and $y(t)$ is a normalized version of the cross-power spectral density, $S_{\rm xy}(f)$. Its magnitude is defined as:

$$\gamma(f) = \frac{|S_{\rm xy}(f)|}{\sqrt{S_{\rm xx}(f)S_{\rm yy}(f)}}, \quad \gamma(f) \in [0,1] \tag{1}$$

$$S_{\rm xy}(f) = \mathcal{F}_{\tau\to f}\left\{ \mathtt{E}\left[x(t)y^*(t-\tau)\right] \right\} \tag{2}$$

where $\mathcal{F}\{\cdot\}$ and $\mathtt{E}[\cdot]$ stand for the Fourier transform and the expectation operator, respectively. The magnitude of spectral coherence is one in the spectral ranges in which $x(t)$ and $y(t)$ are related by a linear time-invariant system and zero in the spectral ranges in which $x(t)$ and $y(t)$ are uncorrelated, i.e., when $S_{\rm xy}(f) = 0$ [1], [16].

The TFC function quantifies the strength of the local coupling between nonstationary processes and can be defined as [16], [17]

$$\gamma(t,f) = \frac{|S_{\rm xy}(t,f)|}{\sqrt{S_{\rm xx}(t,f)S_{\rm yy}(t,f)}}, \quad \gamma(t,f) \in [0,1] \tag{3}$$

where $S_{\rm xy}(t,f)$ stands for some nonstationary cross spectrum. The nonstationary spectrum used in (3) does not have a unique definition. The Wigner–Ville spectrum (WVS), defined as the Fourier transform of a nonstationary cross-correlation function [18]

$$S_{\rm xy}(t,f) = \mathcal{F}_{\tau\to f}\left\{ \mathtt{E}\left[x\left(t+\frac{\tau}{2}\right) y^*\left(t-\frac{\tau}{2}\right)\right]\right\} \tag{4}$$

can be seen as a natural extension of the cross-power spectral density in a nonstationary context. It can be shown that, under mild conditions, the WVS is equal to the ensemble average of the Wigner–Ville distributions, $W_{\rm xy}(t,f)$, of the realizations of the processes [18]

$$S_{\rm xy}(t,f) = \mathtt{E}\left[W_{\rm xy}(t,f)\right] \tag{5}$$

$$W_{\rm xy}(t,f) = \mathcal{F}_{\tau\to f}\left\{ x\left(t+\frac{\tau}{2}\right) y^*\left(t-\frac{\tau}{2}\right)\right\}. \tag{6}$$

When only one observed realization is available, as in single-trial analysis, $S_{\rm xy}(t,f)$ should be estimated by replacing $\mathtt{E}[W_{\rm xy}(t,f)]$ with local averaging

$$\hat{S}_{\rm xy}(t,f;\phi) = W_{\rm xy}(t,f) \otimes \phi(t,f) \tag{7}$$

where $\otimes$ represents the convolution on t and f, and $\phi(t,f)$ is a smoothing function, which, given (3), should guarantee the positiveness of the spectra. In this paper, two different estimators of $S_{\rm xy}(t,f)$ (4) are considered to estimate the coherence function $\gamma(t,f)$, namely, the SPWVD and the MTSP.

A. Time-Frequency Coherence by Smoothed Pseudo-Wigner-Ville Distribution (SPWV-TFC)

The SPWVD is a member of Cohen's class and corresponds to the particular case in which $\phi(t,f)$ is a separable function. It is defined as

$$\begin{aligned}
\hat{S}^{\rm W}_{\rm xy}(t,f) &= W_{\rm xy}(t,f) \otimes \phi(t,f) = \mathcal{F}_{(\nu,\tau)\to(t,f)}\left\{A_{\rm xy}(\nu,\tau)\Phi(\nu,\tau)\right\} \\
A_{\rm xy}(\nu,\tau) &= \mathcal{F}_{t\to\nu}\left\{ x\left(t+\frac{\tau}{2}\right) y^*\left(t-\frac{\tau}{2}\right)\right\} \\
\Phi(\nu,\tau) &= \mathcal{F}^{-1}_{(t,f)\to(\nu,\tau)}\{\phi(t,f)\}
\end{aligned} \tag{8}$$

where $\mathcal{F}_{(\nu,\tau)\to(t,f)}$ is the Fourier transform operator, used to pass from the ambiguity function domain to the TF domain, and $A_{\rm xy}(\nu,\tau)$ is the cross-ambiguity function of signals $x(t)$ and $y(t)$. The presence of residual interference terms [16], [19] in the SPWVD may cause $\hat{\gamma}(t,f) \notin [0,1]$. Indeed, the Janssen's interference formula [19]

$$|W_{\rm xy}(t,f)|^2 = \iint W_{\rm xx}\left(t+\frac{\tau}{2}, f+\frac{\nu}{2}\right) W_{\rm yy}\left(t-\frac{\tau}{2}, f-\frac{\nu}{2}\right) d\tau d\nu \tag{9}$$

shows that for some TF point (t_0, f_0), it is possible to have $|W_{\rm xy}(t_0,f_0)| \neq 0$ while $W_{\rm xx}(t_0,f_0) = W_{\rm yy}(t_0,f_0) \approx 0$, and consequently $\hat{\gamma}(t_0,f_0) > 1$. To obtain coherence estimates that range between 0 and 1, the kernel should completely suppress the interference terms [16]. A necessary, but not sufficient, condition to have coherence estimates bounded between 0 and 1 is the positiveness of the auto-spectra. As long as the degree of TF filtering is strong enough, TF coherence by SPWVD (SPWV-TFC) is obtained as

$$\hat{\gamma}^{\rm W}(t,f) = \frac{\left|\hat{S}^{\rm W}_{\rm xy}(t,f)\right|}{\sqrt{\hat{S}^{\rm W}_{\rm xx}(t,f)\hat{S}^{\rm W}_{\rm yy}(t,f)}}. \tag{10}$$

To suppress the interference terms, a simplified version of the multiform-tiltable exponential kernel [20] is used

$$\Phi(\nu,\tau) = \exp\left\{ -\pi\left[\left(\frac{\nu}{\nu_0}\right)^2 + \left(\frac{\tau}{\tau_0}\right)^2\right]^{2\lambda}\right\}. \tag{11}$$

In the ambiguity function domain, the isocontours of (11) are ellipses whose eccentricities depend on parameters ν_0 and τ_0. Parameters ν_0 and τ_0 are used to change the length of the ellipse axes aligned along ν (the degree of time filtering) and τ (the degree of frequency filtering), respectively. The parameter λ sets the roll-off of the filter as well as the size of the tails of the kernel.

The resolution of the SPWVD is given by the shape of the separable kernel function. The spreading introduced by the kernel is assessed by estimating the SPWVD of a Dirac impulse and of a complex exponential, whose ideal TF representations are straight lines in frequency and time direction, respectively. This is shown by the following expressions: for $x(t) = \delta(t-t_0)$, $\hat{S}^{\rm W}_{\delta\delta}(t,f) = \int \phi(t-t_0, f-f')df'$; for $x(t) = e^{i2\pi f_0 t}$, $\hat{S}^{\rm W}_{\rm ee}(t,f) = \int \phi(t-t', f-f_0)dt'$. Temporal and spectral resolutions are quantified by the full width at half maximum ($\Delta^{\rm m}$), and by the full width at $a\%$ of the total area

($\Delta^{(a\%)}$) of the kernel function or, alternatively, of $\hat{S}^{W}_{\delta\delta}(t, f_0)$ and $\hat{S}^{W}_{ee}(t_0, f)$, respectively (examples are given in Fig. 4 and comments in Section IV).

B. Time-Frequency Coherence by Multitaper Spectrogram (MTSP-TFC)

A spectrogram is another estimator of the Wigner–Ville spectrum (4), defined as [18], [21]

$$\hat{S}^{S}_{xy}(t,f)=\left[\mathcal{F}_{\tau\to f}\left\{x(\tau)h(\tau-t)\right\}\right]\left[\mathcal{F}_{\tau\to f}\left\{y(\tau)h(\tau-t)\right\}\right]^{*}. \tag{12}$$

The spectrogram is a member of Cohen's class, estimated by using (7) and replacing $\phi(t, f)$ with the Wigner–Ville distribution of $h(t)$, $W_{hh}(t, f)$. The advantages of spectrogram are the reduced level of interference terms and that it is non-negative. Shortcomings are related to the poor joint TF resolution given by $h(t)$. The impossibility of independently adjusting the smoothing in time and frequency leads to the well known tradeoff: The better a signal component is localized in time (or frequency), the worse it is localized in frequency (or time). Moreover, spectrograms, as defined in (12), cannot be used in single-trial coherence analysis since $|\hat{S}^{S}_{xy}(t, f)|^2 = \hat{S}^{S}_{xx}(t, f)\hat{S}^{S}_{yy}(t, f)$; consequently, $\hat{\gamma}(t, f) = 1$. In a statistical sense, the spectrogram is an inconsistent estimator of the WVS, with a variance in the order of the squared WVS [18]. The MTSP, which is the extension of a methodology proposed to improve the estimation of the power spectral density [22], was introduced to improve the bias-variance tradeoff of a traditional spectrogram [23], [24]. The MTSP is computed by averaging different spectrograms, obtained by using a set of orthogonal windows $h_k(t)$

$$\hat{S}^{S}_{xy}(t,f;K) = \frac{1}{K}\sum_{k=1}^{K}\left[\mathcal{F}_{\tau\to f}\left\{x(\tau)h_k(\tau-t)\right\}\right] \times\left[\mathcal{F}_{\tau\to f}\left\{y(\tau)h_k(\tau-t)\right\}\right]^{*} \tag{13}$$

where $h_k(t)$ are Hermite functions, that are used because they are optimally concentrated in a circular TF region [13]. They are estimated as [24]

$$h_k(t) = e^{-\frac{t^2}{2}}\mathcal{H}_k(t)/\sqrt{\pi^{\frac{1}{2}}2^k k!} \tag{14}$$

where $\mathcal{H}_k(t)$, with $k \in \mathbb{N}$, stands for Hermite polynomials, which obey the recursion

$$\mathcal{H}_k(t) = 2t\mathcal{H}_{k-1}(t) - 2(k-2)\mathcal{H}_{k-2}(t), \quad k \geq 2 \tag{15}$$

with the initialization $\mathcal{H}_0(t) = 1$, $\mathcal{H}_1(t) = 2t$.

With only a few Hermite functions (as $K = 4$) the corresponding kernel, $\phi(t, f) = W_{hh}(t, f)$ in (7), is the sum of K Laguerre functions and approximates a "top-hat" function [13], [23] (see Fig. 4 in Section IV). Time and frequency resolutions are quantified by indices Δ^{m} and $\Delta^{(a\%)}$ estimated from the MTSP of a Dirac impulse $\delta(t - t_0)$, $\hat{S}^{S}_{\delta\delta}(t, f_0) = \frac{1}{K}\sum_{k=1}^{K} h_k(t - t_0)^2$, and that of a complex exponential $e^{i2\pi f_0 t}$, $\hat{S}^{S}_{ee}(t_0, f) = \frac{1}{K}\sum_{k=1}^{K} |H_k(f - f_0)|^2$, where $H_k(f)$ is the Fourier transform of $h_k(t)$.

Time-frequency coherence by multitaper spectrogram (MTSP-TFC) is obtained as

$$\hat{\gamma}^{S}(t,f) = \frac{\left|\hat{S}^{S}_{xy}(t,f;K)\right|}{\sqrt{\hat{S}^{S}_{xx}(t,f;K)\hat{S}^{S}_{yy}(t,f;K)}}. \tag{16}$$

C. Statistical Analysis

The local averaging provided by the smoothing function (7), causes the coherence estimates of two uncorrelated signals to be not null. This dependence introduces an uncertainty in the interpretation of the coherence estimates. To reduce this uncertainty and to localize TF regions characterized by a significant coherence level, a hypothesis test is used. The null hypothesis states that two signals $x(t)$ and $y(t)$ are uncorrelated around a point (t_0, f_0). The test consists of the following steps: 1) Generate uncorrelated test signals $\tilde{x}_j(t)$ and $\tilde{y}_j(t)$. 2) Estimate the distribution $\Gamma(t, f) = \{\hat{\gamma}_1(t, f), \ldots, \hat{\gamma}_j(t, f), \ldots\}$, where $\hat{\gamma}_j(t, f)$ is the TFC between the jth realization of test signals $\tilde{x}_j(t)$ and $\tilde{y}_j(t)$. 3) Estimate the threshold $\gamma_{TH}(t, f; \alpha)$, as the $(1 - \alpha)^{th}$ percentile of $\Gamma(t, f)$, where the significance level α represents the probability of wrongly rejecting the null hypothesis. 4) Determine a TF mask $\mathcal{M}(t, f; \alpha)$, which identifies the regions in which the null hypothesis can be rejected

$$\begin{cases} \mathcal{M}(t,f;\alpha) = 1, & \text{if } \hat{\gamma}(t,f) > \gamma_{TH}(t,f;\alpha) \text{ coupling} \\ \mathcal{M}(t,f;\alpha) = 0, & \text{if } \hat{\gamma}(t,f) \leq \gamma_{TH}(t,f;\alpha) \text{ no coupling.} \end{cases} \tag{17}$$

A priori, the threshold function $\gamma_{TH}(t, f; \alpha)$ should depend on α, on the geometry of the kernel and on the spectral properties of the analyzed signals. In this study, a signal dependent and a signal independent threshold functions are used.

1) Signal Independent Threshold (SITH): Test signals are white noises. In this case, the threshold $\gamma^{SI}_{TH}(t, f; \alpha)$ will depend only on the kernel and is expected to be constant over the TF domain.

2) Signal Dependent Threshold (SDTH): The estimation of SDTH involves three steps: 1) Estimate $\gamma^{x}_{TH}(t, f)$ from $\Gamma_x(t, f) = \{\hat{\gamma}_{x,1}(t, f), \ldots, \hat{\gamma}_{x,j}(t, f), \ldots\}$, where $\hat{\gamma}_{x,j}(t, f)$ is the TFC between signal $x(t)$ and a the j-th realization of a white noise. 2) Estimate $\gamma^{y}_{TH}(t, f)$ from $\Gamma_y(t, f) = \{\hat{\gamma}_{y,1}(t, f), \ldots, \hat{\gamma}_{y,j}(t, f), \ldots\}$, where $\hat{\gamma}_{y,j}(t, f)$ is the TFC between signal $y(t)$ and a the j-th realization of a white noise. 3) SDTH is obtained as $\gamma^{SD}_{TH}(t, f; \alpha) = \max[\gamma^{X}_{TH}(t, f; \alpha), \gamma^{Y}_{TH}(t, f; \alpha)]$.

III. MATERIALS

A. Simulation Study

Signals whose dynamics depend on the modulation of the autonomic nervous system, such as heart rate variability, arterial pressure variability, and respiratory signal, could be modeled as the real part of the sum of complex exponentials showing both

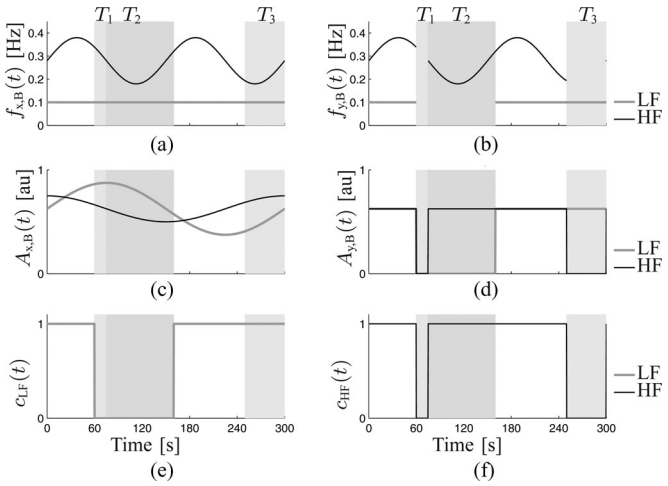

Fig. 1. Simulation study. (a)–(d): Instantaneous frequencies $f_{\mathrm{k,B}}(t)$, with $k \in \{x, y\}$ and B$\in \{LF, HF\}$ and amplitudes $A_{\mathrm{k,B}}(t)$, of LF and HF components of signals $x(t)$ and $y(t)$ (18). (e), (f) Theoretical coherence patterns $c_{\mathrm{B}}(t)$ in LF and HF bands. Shadowed areas correspond to interval of uncoupling in both LF and HF (T_1), in LF (T_2) and in HF (T_3).

amplitude and frequency modulation, embedded in noise

$$\begin{cases} x(t) = A_{\mathrm{x,LF}}(t)e^{i\theta_{\mathrm{x,LF}}(t)} + A_{\mathrm{x,HF}}(t)e^{i\theta_{\mathrm{x,HF}}(t)} + \xi_{\mathrm{x}}(t) \\ y(t) = A_{\mathrm{y,LF}}(t)e^{i\theta_{\mathrm{y,LF}}(t)} + A_{\mathrm{y,HF}}(t)e^{i\theta_{\mathrm{y,HF}}(t)} + \xi_{\mathrm{y}}(t) \end{cases} \tag{18}$$

where $\xi_{\mathrm{x}}(t)$ and $\xi_{\mathrm{y}}(t)$ are two independent white Gaussian noises, and subscripts LF and HF stand for low frequency range [0.04, 0.15 Hz] and high frequency range [0.15, 0.4 Hz], respectively. Instantaneous phases and frequencies are related by $f(t) = (d\theta(t)/dt)/(2\pi)$. The time-courses of the signal components used in this simulation are shown in Fig. 1(a)–(d). Signals $x(t)$ and $y(t)$ can be seen as locally coupled since their spectral components share the same instantaneous frequencies and their amplitudes vary slowly. They are expected to be coupled over the entire TF domain except in three localized regions. During T_1 (lasting 15 s), both LF and HF components are uncoupled because $A_{\mathrm{y,LF}}(T_1) = A_{\mathrm{y,HF}}(T_1) = 0$. During T_2 (85 s), the signals are uncoupled in LF because $A_{\mathrm{y,LF}}(T_2) = 0$, while during T_3 (50 s), the signals are uncoupled in HF because $A_{\mathrm{y,HF}}(T_3) = 0$. The correct localization of the TF regions where signals are coupled/uncoupled is challenging since both instantaneous frequencies and amplitudes of the signals are time-varying. From a physiological viewpoint, the time-courses of the instantaneous frequencies of HF components, $f_{\mathrm{x,HF}}(t)$ and $f_{\mathrm{y,HF}}(t)$, cover the range of possible respiratory frequencies observed in many autonomic tests, and it may correspond to a pattern observed during some respiratory disorders, such as periodic breathing. From a theoretical viewpoint, the tracking of time-varying spectral components characterized by sinusoidal frequency modulation is challenging due to the high level of inner interference terms that characterizes signals with such a modulation [19]. Moreover, $f_{\mathrm{x,HF}}(t)$ and $f_{\mathrm{y,HF}}(t)$ reach values as low as 0.18 Hz (10.8 breaths/min), mimicking slow breathing. In this situation, separating LF and HF components requires high resolution.

TABLE I
SIMULATION STUDY: DETECTION SCHEME

Test outcome	Gold standard $c_{\mathrm{B}}(t_0) = 1$	Gold standard $c_{\mathrm{B}}(t_0) = 0$
$\mathcal{M}(t_0, f_{\mathrm{B}}(t_0); \alpha) = 1$	True Positive (TP)	False Positive (FP)
$\mathcal{M}(t_0, f_{\mathrm{B}}(t_0); \alpha) = 0$	False Negative (FN)	True Negative (TN)

The capability of the TFC estimators to track the changes described above is quantified in terms of accuracy. Gold standards are represented by indices $c_{\mathrm{LF}}(t)$ and $c_{\mathrm{HF}}(t)$ which, by definition, are equal to 1 when signals are coupled, and 0 when signals are uncoupled at $f_{\mathrm{LF}}(t)$ and $f_{\mathrm{HF}}(t)$, respectively [see Fig. 1(e)–(f)]. At each point $(t_0, f_{\mathrm{B}}(t_0))$, with $B = \{\mathrm{LF,HF}\}$, outcomes are classified as shown in Table I. According to this scheme, a low sensitivity (or specificity) corresponds to the identification of intervals of local coupling (or uncoupling) shorter than the true ones. Accuracy is given by AC=(TP+TN)/(TP+TN+FP+FN).

B. Physiological Study

Fourteen healthy subjects (aged 29 $\pm$ 3 years) underwent a tilt table test. The protocol consisted of 4 min in early supine position (T_{es}), 5 min head-up tilted to an angle of 70° (T_{ht}), and 4 min back to later supine position (T_{ls}) [25]. The ECG and respiratory signals were recorded using the BIOPAC MP 150 system with a sampling frequency of 1 kHz and 125 Hz, respectively. The respiratory signal was recorded through a strain gauge transducer. The pressure signal was recorded at the finger by the Finometersystem with a sampling frequency of 250 Hz, and without correction for the hydrostatic gradient change during tilt. Beats from ECG and pulses from the pressure signal were detected to generate RR, pulse interval and systolic arterial pressure time series. During the procedure, the Finometer was recalibrated at the beginning of T_{ht} and T_{ls}. The recalibration took few seconds and introduced artifacts which were detected and corrected by interpolation. The series were subsequently resampled at 4 Hz, and RRV, PIV from the finger pressure measurement and SAPV signals were obtained by high-pass filtering the corresponding series with a cut-off frequency of 0.03 Hz. The degree of coupling between RRV and RESP, RRV and SAPV, and RRV and PIV was assessed.

IV. RESULTS

A. Relation Between Degree of Time-Frequency Filtering and Coherence Estimates

The relation between the mean value of the signal independent threshold function, $\overline{\gamma_{\mathrm{TH}}^{\mathrm{SI}}}$, and the TF resolution is shown in Fig. 2. $\overline{\gamma_{\mathrm{TH}}^{\mathrm{SI}}}$ was obtained by collecting the TFC of 250 couples of white noise, and with $\alpha = 5\%$. This figure reveals the strong dependence of coherence estimates on the geometry of the kernel, and confirms the need of a statistical test to assess the local coupling. Depending on the kernel, $\overline{\gamma_{\mathrm{TH}}^{\mathrm{SI}}}$ can be as high as 0.9, being higher for lower degree of smoothing. This implies that, without an appropriate statistical test, it is easy to wrongly detect local coupling. For each combination of time and frequency resolution,

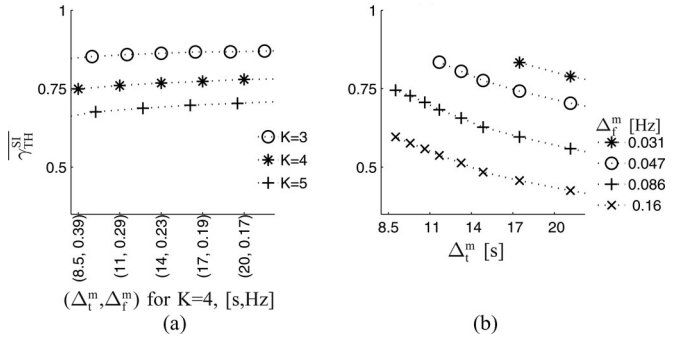

Fig. 2. Signal independent thresholds $\overline{\gamma_{\mathrm{TH}}^{\mathrm{SI}}}$, with $\alpha = 5\%$, corresponding to different TF resolutions. (a) MTSP-TFC: Results are obtained by using $K = \{3,4,5\}$ Hermite functions. (b) SPWV-TFC: Time resolution $\Delta_{\mathrm{t}}^{\mathrm{m}}$ is reported on the horizontal axis, frequency resolution $\Delta_{\mathrm{f}}^{\mathrm{m}}$ is coded by different symbols.

the coefficient of variation of $\gamma_{\mathrm{TH}}^{\mathrm{SI}}(t,f)$ never exceeded 3%, and $\overline{\gamma_{\mathrm{TH}}^{\mathrm{SI}}}$ stabilized having processed 75 noise realizations. This shows that the threshold is uniform over the TF domain and suggests that only few pairs of white noises are necessary to reliably estimate the threshold value. Fig. 2(a) shows that $\overline{\gamma_{\mathrm{TH}}^{\mathrm{SI}}}$ estimated by MTSP decreased by increasing the number of tapers K, while for a given number of tapers, $\overline{\gamma_{\mathrm{TH}}^{\mathrm{SI}}}$ was almost independent of the different combinations of time and frequency resolutions. This is likely due to the fact that the TF support of the kernel associated with different $h_{\mathrm{k}}(t)$ is approximately the same (when the width of $h_{\mathrm{k}}(t)$ increases, the width of $|H_{\mathrm{k}}(f)|$ decreases). Fig. 2(b) shows that $\overline{\gamma_{\mathrm{TH}}^{\mathrm{SI}}}$ estimated by SPWVD was inversely related to the degree of TF smoothing. Only the combinations of time and frequency smoothing that gave $\hat{\gamma}^{\mathrm{W}}(t,f) \in [0,1]$ are shown. In this example, the finest resolutions of the SPWVD were: $(\Delta_{\mathrm{t}}^{\mathrm{m}}, \Delta_{\mathrm{f}}^{\mathrm{m}}) \approx$(18 s, 0.031 Hz), (12 s, 0.047 Hz), (9 s, 0.086 Hz). For the same $\Delta_{\mathrm{t}}^{\mathrm{m}}$, the MTSP with $K = 4$ gave much lower $\Delta_{\mathrm{f}}^{\mathrm{m}}$, being $(\Delta_{\mathrm{t}}^{\mathrm{m}}, \Delta_{\mathrm{f}}^{\mathrm{m}}) \approx$(18 s, 0.203 Hz), (12 s, 0.305 Hz), (9 s, 0.402 Hz). Fig. 3 represents the signal dependent threshold, $\gamma_{\mathrm{TH}}^{\mathrm{SD}}(t,f)$, corresponding to signals described in Fig. 1, characterized by SNR equal to 20, 5, and -10 dB. Thresholds were obtained by using, for both $\Gamma_{\mathrm{x}}(t,f)$ and $\Gamma_{\mathrm{y}}(t,f)$, 250 realizations of test signals, and $\alpha = 5\%$. Threshold $\gamma_{\mathrm{TH}}^{\mathrm{SD}}(t,f)$ estimated by SPWVD reflects the narrow band structure of the signals, at least for high SNR level, while $\gamma_{\mathrm{TH}}^{\mathrm{SD}}(t,f)$ estimated by MTSP is constant over the TF domain. In the following, given that for MTSP $\gamma_{\mathrm{TH}}^{\mathrm{SD}}(t,f) \approx \gamma_{\mathrm{TH}}^{\mathrm{SI}}(t,f)$, the statistical test for MTSP-TFC will be performed by SITH only.

B. Simulation Study

Taking into account the time-course of the spectral components of $x(t)$ and $y(t)$ shown in Fig. 1, one could require to use a smoothing that gives $\Delta_{\mathrm{t}}^{\mathrm{m}} = 7.5$ s and $\Delta_{\mathrm{f}}^{\mathrm{m}} = 0.04$ Hz. These values correspond to half the duration of the shortest decorrelating interval, and half the minimal spectral distance between LF and HF component. The parameters of the MTSP and the SPWVD that gave resolutions close to these values were chosen. The TF spectra of a Dirac impulse, $x(t) = \delta(t - t_0)$, and of a complex exponential, $x(t) = e^{i2\pi f_0 t}$, estimated by SPWVD and MTSP used in the simulation study, are shown in Fig. 4.

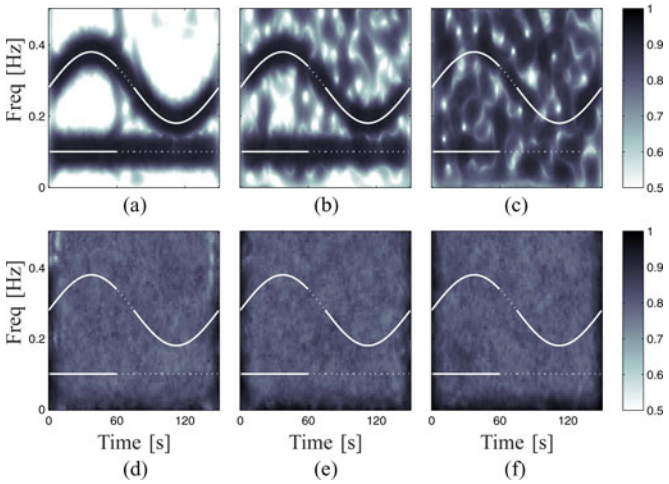

Fig. 3. Signal-dependent threshold $\gamma_{\mathrm{TH}}^{\mathrm{SD}}(t,f)$ for (a)–(c) SPWV-TFC and (d)–(f) MTSP-TFC. Statistical level $\alpha = 5\%$. Signals are of the type described in Fig. 1. Instantaneous frquencies of $x(t)$ and $y(t)$ are reported in dotted and continuous line, respectively. (a) SNR = 20 dB. (b) SNR = 5 dB. (c) SNR = -10 dB. (d) SNR = 20 dB (e) SNR = 5 dB (f) SNR = -10 dB.

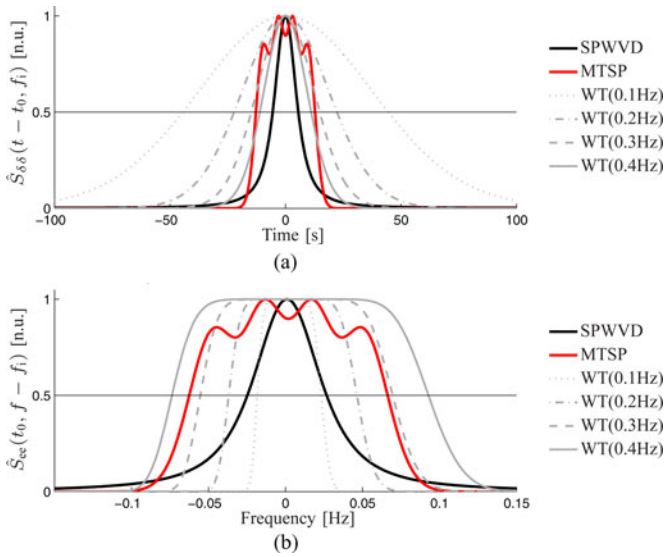

Fig. 4. Time-frequency representations of: (a) Dirac impulse $x(t) = \delta(t - t_0)$, $\hat{S}_{\delta\delta}(t - t_0, f_{\mathrm{i}})$; (b) complex exponential $x(t) = e^{i2\pi f_{\mathrm{i}} t}$, $\hat{S}_{\mathrm{ee}}(t_0, f - f_{\mathrm{i}})$. The SPWVD and MTSP are the same $\forall f$, while the wavelet transform (WT) is estimated for $f_{\mathrm{i}} \in \{0.1, 0.2, 0.3, 0.4\}$ Hz. (a) Spreading in time. (b) Spreading in frequency.

For comparison, TF spectra estimated by WT are also shown. Wavelet spectra were obtained by using a specific toolbox for the estimation of wavelet coherence [26]. As suggested in [10], Morlet wavelet with $\omega_0 = 20$ is used, and a further smoothing is applied to obtain spectra that can be used in the estimation of wavelet coherence [10], [26]. Given that the resolution of the WT depends on frequency, the spectra of the Dirac impulse and of complex exponentials $x(t) = e^{i2\pi f_{\mathrm{i}} t}$ were estimated for $f_{\mathrm{i}} \in \{0.1, 0.2, 0.3, 0.4\}$ Hz. From the spectra shown in Fig. 4, indices Δ^{m} and $\Delta^{(\mathrm{a}\%)}$ were estimated, and are reported in Table II. The SPWVD was characterized by much better resolution than the MTSP: $\Delta_{\mathrm{t}}^{\mathrm{m}}$ and $\Delta_{\mathrm{f}}^{\mathrm{m}}$ of the SPWVD were

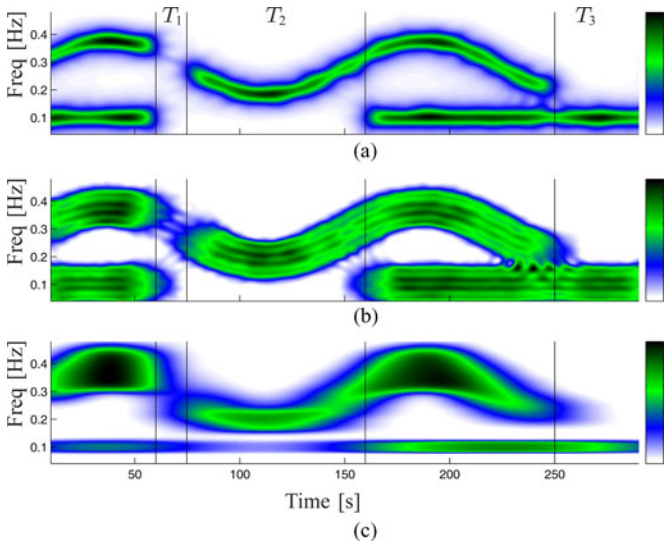

Fig. 5 Time-frequency spectra of one realization of signal $x_2(t)$, characterized by SNR=10 dB, used in the simulation study. (a) SPWVD, $\hat{S}^{\mathrm{W}}_{\mathrm{xx}}(t,f)$; (b) MTSP, $\hat{S}^{\mathrm{S}}_{\mathrm{xx}}(t,f)$, with $K=4$; (c) Wavelet transform. The kernels used to estimate these spectra are the same as those used in Fig. 5.

about half $\Delta^{\mathrm{m}}_{\mathrm{t}}$ and $\Delta^{\mathrm{m}}_{\mathrm{f}}$ of the MTSP. Nevertheless, the Hermite functions, being $\Delta^{(90\%)}/\Delta^{\mathrm{m}} < 1$ (i.e., $\frac{1}{4}\sum_1^4 |h_{\mathrm{k}}(t)|^2$ and $\frac{1}{4}\sum_1^4 |H_{\mathrm{k}}(f)|^2$ had practically no tails), made the smoothing of the MTSP well concentrated in the TF domain. The kernel used in the calculation of the SPWVD, was characterized by $\Delta^{(90\%)}/\Delta^{\mathrm{m}} \approx 3$. The presence of tails in the kernel used to estimate the SPWVD (11) is necessary to find a good compromise between the elimination of the interference terms and the TF resolution. The SPWVD was also characterized by much better resolution than the WT, except for frequency resolution at $f = 0.1$ Hz, for which $\Delta^{\mathrm{m}}_{\mathrm{f}}$ of WT was slightly lower than $\Delta^{\mathrm{m}}_{\mathrm{f}}$ of SPWVD.

Fig. 5 depicts the TF spectra, estimated by SPWVD, MTSP, and WT, of a signal used in the simulation study characterized by SNR=10 dB. The kernels used in this example were the same as those used in Fig. 4. It is shown that the SPWVD gave a more accurate localization of the time-varying spectral components of the signals. For $f \approx 0.1$ Hz, the SPWVD and WT were characterized by similar frequency resolution. However, around this frequency, the SPWVD offered a fine temporal resolution (see also Fig. 4 and table II), while the WT gave a very poor representation of the temporal changes of the LF component, which did not vanish during T_1 and T_2. Furthermore, in the WT, the bandwidth of the HF component is much wider than the bandwidth of the LF one. However, this does not reflect the "real" structure of the signals, but it is due to the frequency-dependent resolution of WT.

In Fig. 6, the maps of the significance level of the local coupling between a couple of representative signals are shown for different SNR. These kinds of maps provide a useful alternative representation of the results of single-trial coherence analysis. Regions in which the coupling is not significant (i.e., $\alpha > 5\%$) are reported in white, while those in which the coupling is significant (i.e., $\alpha < 5\%$) are reported in gray scale, with intensities that depend on the significance level α. For instance, regions where coherence estimates are higher than the threshold corresponding to $\alpha = 0.1\%$ are reported in black. White and black lines represent the regions where signals are coupled, i.e., $c_{\mathrm{B}}(t) = 1$, and uncoupled, i.e., $c_{\mathrm{B}}(t) = 0$, respectively. The SPWVD localized coherence changes better, due to higher resolution both in time and frequency. This led to the correct estimation of the duration of T_1, T_2, and T_3, and to separate the LF and HF components even when they were close. Results shown in Fig. 6(c), obtained by comparing $\hat{\gamma}^{\mathrm{W}}(t,f)$ to the SDTH, matched the ideal TFC distribution characterized by a coherence level that is not significant only in well-localized TF regions: during T_1 in both LF and HF bands, during T_2 in LF band, and during T_3 in HF band. In Fig. 6(g), it is shown that for an SNR as low as 0 dB, the MTSP-TFC estimator identifies larger regions characterized by local coupling.

TABLE II
SIMULATION STUDY—TF RESOLUTION

	Time Resolution (s)		Freq Resolution (Hz)	
	$\Delta^{\mathrm{m}}_{\mathrm{t}}$	$\Delta^{(90\%)}_{\mathrm{t}}$	$\Delta^{\mathrm{m}}_{\mathrm{f}}$	$\Delta^{(90\%)}_{\mathrm{f}}$
SPWVD	11.1	39.5	0.051	0.185
MTSP (K=4)	25.6	25.1	0.129	0.127
WT (0.1Hz)	89.0	124.2	0.041	0.042
WT (0.2Hz)	44.5	64.2	0.083	0.082
WT (0.3Hz)	29.6	42.8	0.124	0.122
WT (0.4Hz)	22.2	32.1	0.166	0.162

Global results, given in terms of accuracy, are shown in Fig. 7. In these graphics, the influence of noise, type of threshold, and significance level are assessed. For each combination of these parameters, 50 pairs of signals were processed. These results show that: 1) Coherence by SPWVD is characterized by higher accuracy than coherence by MTSP; for example, for SNR≥ 0 and $\alpha = 0.1\%$, the global accuracy of $\hat{\gamma}^{\mathrm{W}}(t,f)$, estimated by averaging results obtained in LF and HF bands, was more than 11.8% higher than the accuracy of $\hat{\gamma}^{\mathrm{S}}(t,f)$. 2) Accuracy of the $\hat{\gamma}^{\mathrm{W}}(t,f)$ was very high for SNR ≥ 5 dB (AC $> 96.9\%$, averaging results in LF and HF ranges). 3) The differences between the accuracy of $\hat{\gamma}^{\mathrm{W}}(t,f)$ and $\hat{\gamma}^{\mathrm{S}}(t,f)$ decreased by increasing α. (4) In $\hat{\gamma}^{\mathrm{W}}(t,f)$, the use of signal dependent instead of signal independent thresholds improved the accuracy, but only for high SNR.

C. Physiological Study

As an illustrative example, the TF distribution of the RRV and SAPV signals from a healthy subject (male, 27 years old) undergoing a tilt table test is shown in Fig. 8(a)–(d). From visual inspection, it is already possible to detect some correlations between the nonstationary structures of the signals. The resolution was $(\Delta^{\mathrm{m}}_{\mathrm{t}}, \Delta^{\mathrm{m}}_{\mathrm{f}}) = (12\ \mathrm{s}, 0.041\ \mathrm{Hz})$ for the SPWVD and (26.5s, 0.12 Hz) for the MTSP with $K = 4$. At the beginning of the head-up tilt (epoch T_{ht}), the instantaneous LF power of the RRV and SAPV signals quickly increased and maintained high value for about one minute. During the remaining part of T_{ht}, the instantaneous LF power first decreased and then increased until supine position was restored. The component related to respiration was more clearly represented in the SAPV

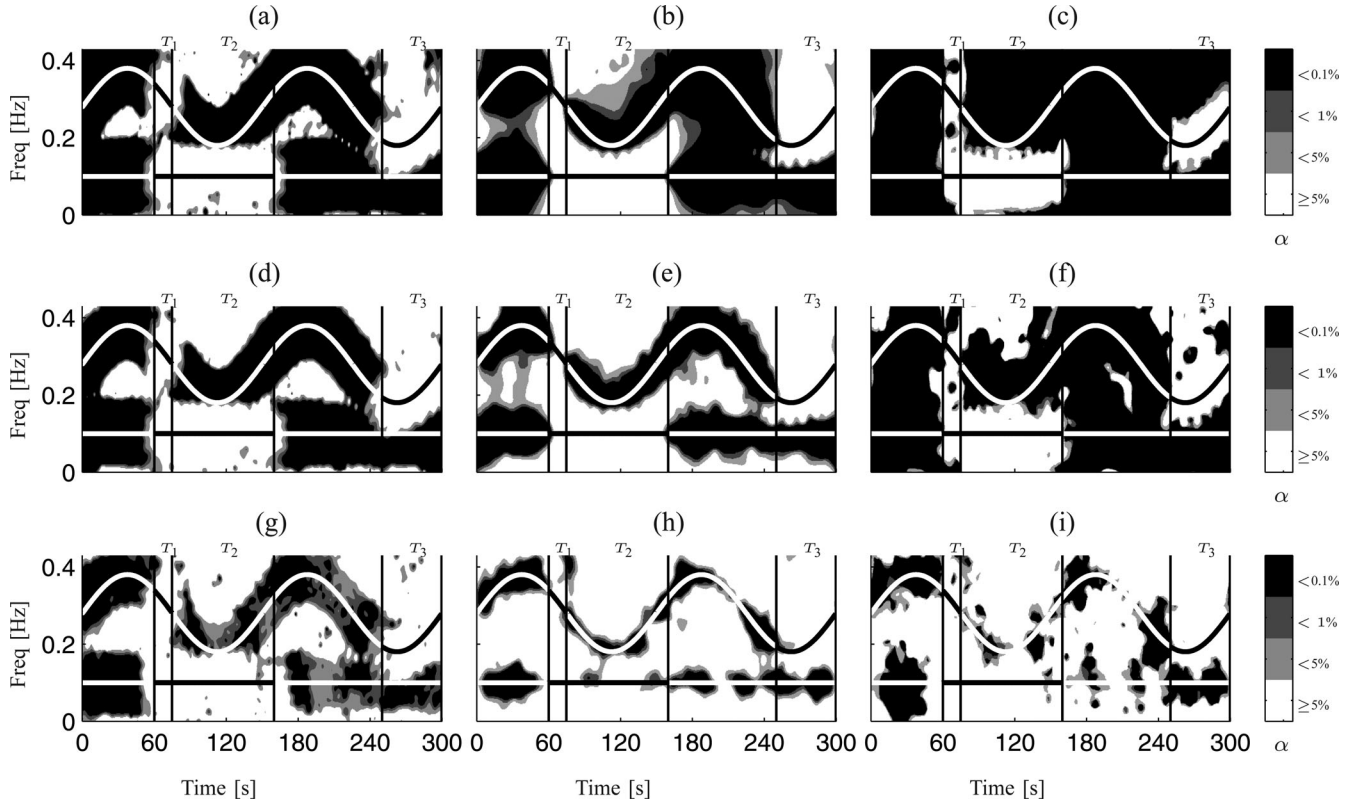

Fig. 6. Simulation study: Single-trial analysis. TF maps of the statistical significance level. First column: MTSP-TFC with SITH; second column: SPWV-TFC with SITH; third column: SPWV-TFC with SDTH; upper (a)–(c), middle (d)–(f), and lower (g)–(i) graphics represent cases of SNR of 20 dB, 10 dB, and 0 dB, respectively. Black and white lines represent regions characterized by presence and lack of coupling. (a) $\hat{\gamma}^{\mathrm{S}}(t,f) \geq \gamma^{\mathrm{SI}}_{\mathrm{TH}}(t,f;\alpha)$ [20 db]. (b) $\hat{\gamma}^{\mathrm{W}}(t,f) \geq \gamma^{\mathrm{SI}}_{\mathrm{TH}}(t,f;\alpha)$ [20 db]. (c) $\hat{\gamma}^{\mathrm{W}}(t,f) \geq \gamma^{\mathrm{SD}}_{\mathrm{TH}}(t,f;\alpha)$ [20 db]. (d) $\hat{\gamma}^{\mathrm{S}}(t,f) \geq \gamma^{\mathrm{SI}}_{\mathrm{TH}}(t,f;\alpha)$ [10 db]. (e) $\hat{\gamma}^{\mathrm{W}}(t,f) \geq \gamma^{\mathrm{SI}}_{\mathrm{TH}}(t,f;\alpha)$ [10 db]. (f) $\hat{\gamma}^{\mathrm{W}}(t,f) \geq \gamma^{\mathrm{SD}}_{\mathrm{TH}}(t,f;\alpha)$ [10 db]. (g) $\hat{\gamma}^{\mathrm{S}}(t,f) \geq \gamma^{\mathrm{SI}}_{\mathrm{TH}}(t,f;\alpha)$ [0 db]. (h) $\hat{\gamma}^{\mathrm{W}}(t,f) \geq \gamma^{\mathrm{SI}}_{\mathrm{TH}}(t,f;\alpha)$ [0 db]. (i) $\hat{\gamma}^{\mathrm{W}}(t,f) \geq \gamma^{\mathrm{SD}}_{\mathrm{TH}}(t,f;\alpha)$ [0 db].

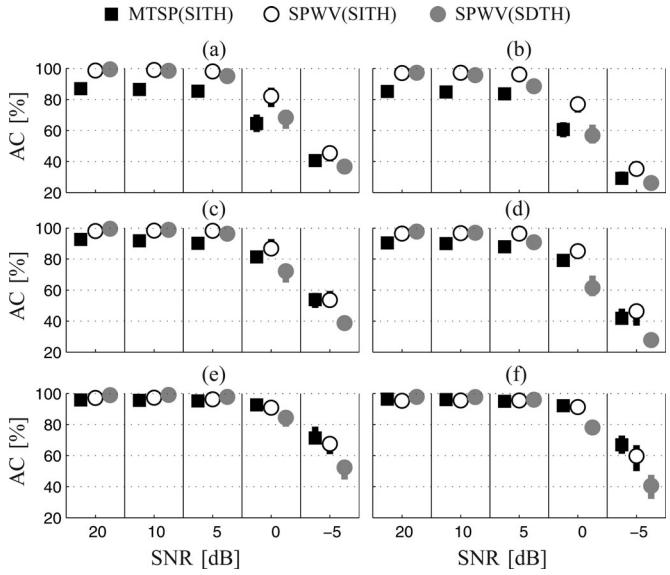

Fig. 7. Simulation study: Global results. Accuracy in the localization of TF regions where signal components are coupled. Fifty pairs of signals $x(t)$ and $y(t)$, characterized by different SNRs are processed and results are given as the 25th, 50th, and 75th percentiles. Right and left panels concern LF and HF components. From top to bottom: Thresholds used in the statistical analysis are associated to a significance level α of 0.1%, 1%, and 5%. (a) LF [$\alpha = 0.1\%$]. (b) HF [$\alpha = 0.1\%$]. (c) LF [$\alpha = 1\%$]. (d) HF [$\alpha = 1\%$]. (e) LF [$\alpha = 5\%$]. (f) HF [$\alpha = 5\%$].

than in the RRV signal. During T_{ht}, the respiratory frequency was higher than the traditional upper limit of HF band (0.4 Hz), indicating that in nonstationary conditions, spectral boundaries should be time-varying and respiratory-dependent [27]. The statistical significance of the coupling between RRV–SAPV, shown in Fig. 8(e) and (f), increased during T_{ht}, especially in the LF band. In LF band, the proportional part of the TF plane in which coherence was significant, was 64%, 88%, and 69% during T_{es}, $T_{\mathrm{ht},}$ and T_{ls}, respectively. During T_{ht}, and around the respiratory rate (reported in red line), the significance of $\hat{\gamma}^{\mathrm{W}}(t,f)$ was higher than that of $\hat{\gamma}^{\mathrm{S}}(t,f)$. This is likely due to the finer resolution of the SPWVD, which better characterized the rapid changes of the HF components in both signals.

To characterize the temporal evolution of the local coupling between the spectral components of the signals, the index $\mathcal{C}_{\mathrm{B}}(t)$ was defined as

$$\mathcal{C}_{\mathrm{B}}(t) = \int_{\mathrm{B}} \hat{\gamma}(t,f)\mathcal{M}(t,f)df \Big/ \int_{\mathrm{B}} df; \quad B \in \{\mathrm{LF}, \mathrm{HF}\}. \tag{19}$$

This index takes into account both the spread and the magnitude of the local coupling, averaged in LF and HF spectral bands. The ability to localize changes in the temporal evolution of the coherence between cardiovascular signals was assessed in the example shown in Fig. 9. This graphic shows the LF oscillations of the RRV and SAPV signals, whose TF spectra are shown in

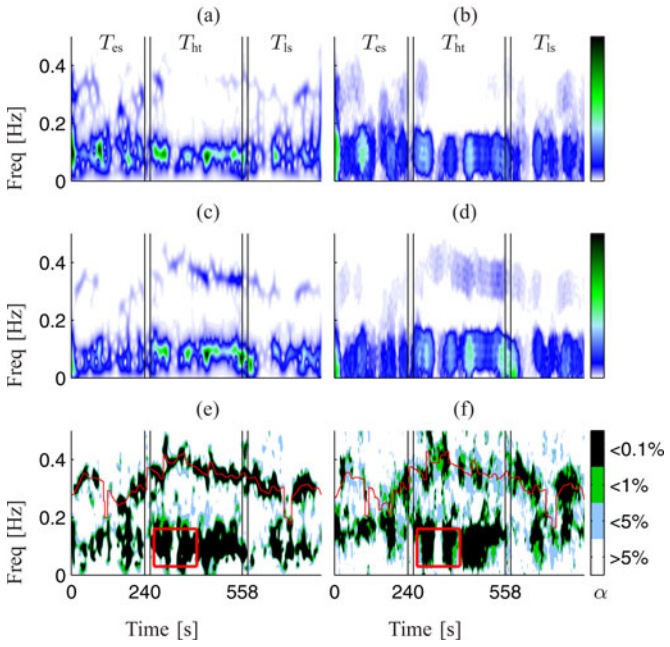

Fig. 8. (a)–(d) Time-frequency spectra estimated by SPWVD, on the left, and by MTSP, on the right, of the RRV and SAPV signals. (e), (f) Coherence by SPWVD and MTSP. Vertical lines mark the supine ($T_{\rm es}$ and $T_{\rm ls}$) and the head-up tilt ($T_{\rm ht}$) positions. The box in (e) and (f) delimited the TF support of oscillations shown in Fig. 9. (a) $\hat{S}^{\rm W}_{\rm xx}(t,f)$ [RRV]. (b) $\hat{S}^{\rm S}_{\rm xx}(t,f)$ [RRV]. (c) $\hat{S}^{\rm W}_{\rm xx}(t,f)$ [SAPV]. (d) $\hat{S}^{\rm S}_{\rm xx}(t,f)$ [SAPV]. (e) $\hat{\gamma}^{\rm W}(t,f)$ [RRV-SAPV]. (f) $\hat{\gamma}^{\rm S}(t,f)$ [RRV-SAPV].

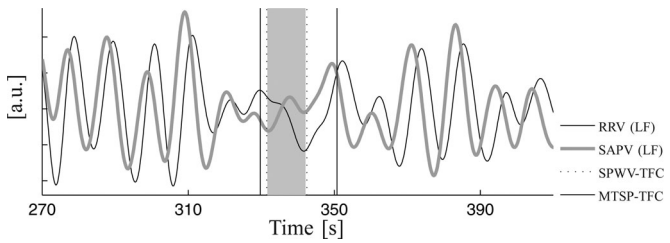

Fig. 9. Low frequency oscillations of the SAPV and RRV signals, obtained by low-pass filtering (see Fig. 8). Shadowed area: Interval of decorrelation. Dashed and continuous vertical lines: Interval of decorrelation detected by the SPWVD and MTSP, respectively.

Fig. 8. These oscillations were obtained by low-pass filtering with a cut-off frequency of 0.16 Hz [see the box of Fig. 8(e) and (f)]. The LF oscillations of the RRV and SAPV signals were highly correlated, except during the interval bounded by two consecutive local minima of the SAPV oscillation, marked by a shadowed area. The intervals during which the coherence, evaluated in the LF range by SPWVD and MTSP, were not statistically significant are bounded by vertical lines. These intervals are those for which $\mathcal{C}_{\rm LF}(t)=0$. As shown in this representative example, SPWVD localized the change in the strength of the local coupling more accurately than MTSP.

The median trend and the interquartile range of $\mathcal{C}_{\rm B}(t)$, estimated among the entire study population, is shown in Fig. 10. Concerning the coupling between RRV–SAPV signals, the head-up tilt provoked a change in $\mathcal{C}_{\rm LF}(t)$ composed of the following phases: 1) instantaneous decrease during the upright movement

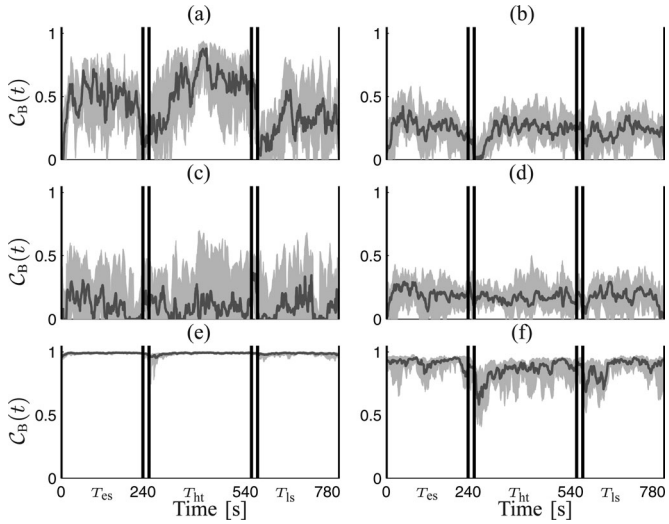

Fig. 10. Global results: Strength and spread of the coupling, $\mathcal{C}_{\rm B}(t)$, between RRV–SAPV (above), RRV–RESP (middle) and RRV–PIV (below), estimated in LF (left) and HF ranges (right). Shadowed area: [25]–75]th percentile of $\mathcal{C}_{\rm B}(t)$, estimated among subjects. Gray lines: Median values. (a) RRV-SAPV [LF]. (b) RRV-SAPV [HF]. (c) RRV-RESP [LF]. (d) RRV-RESP [HF]. (e) RRV-PIV [LF]. (f) RRV-PIV [HF].

of the automatic bed (interval in between vertical lines); 2) fast increase, up to values that are significantly higher than baseline ones (Wilcoxon rank-sum test, $p<0.05$); 3) stabilization around baseline values. In $T_{\rm ls}$, the restoration of the supine position provoked a similar pattern, but characterized by lower $\mathcal{C}_{\rm LF}(t)$. In panel (b), it is shown that, after head-up tilt, $\mathcal{C}_{\rm HF}(t)$ first abruptly decreased and then quickly increased toward baseline values. The increase in the median $\mathcal{C}_{\rm B}(t)$, observed in LF during $T_{\rm ht}$ and $T_{\rm ls}$, and in HF during $T_{\rm ht}$, had similar slopes (4.63, 4.86, and 4.17 $10^{-3}{\rm s}^{-1}$, respectively). The coupling between RRV–RESP signals [panels (c) and (d)] was not significantly affected by the head-up tilt. The coupling between RRV–PIV signals was affected by the postural changes only in HF, while in LF, it was always close to one.

V. Discussion

In this paper, the use of SPWVD and MTSP to reliably estimate the TFC between cardiovascular signals was assessed for the first time. It was shown that the combination of these methods with statistical analysis allows to accurately localize TF regions where the coupling is significant. In contrast with stationary spectral coherence, which quantifies the degree of global linearity, TFC quantifies the degree of local coupling. This is shown in the simulation study, where TFC was significant in a large part of the TF domain, although the signals were not globally linearly related (their amplitudes were not linearly related). This was due to the presence, in both signals, of locally synchronized oscillations.

In the study of cardiovascular control, TFC has many fields of application. For example, it can be used to reveal an impairment of the baroreflex, which results in a low degree of coupling between RRV and SAPV. Time-frequency coherence can be used as a measure of similarity to validate the use of one signal,

and its derived measures, as surrogates of original ones [5]. It can also be used to assess the pertinence of linear (or nonlinear) models to describe the relationship between different signals in the modeling of the cardiovascular system.

A. Statistical Assessment

As for the stationary spectral coherence [1], TFC depends on the parameters used in its calculation. This dependence makes the use of some statistical analysis necessary to assess whether the TFC estimates are significant or not. The problem of interpreting the level of coherence correctly is especially important in nonstationary analysis, since, as shown in Fig. 2, the finer the TF resolution, the higher should be the coherence estimates to be considered as statistically significant. Statistical analysis is based on the point-by-point comparison between coherence estimates and a threshold function. Two thresholds are defined: SITH, which only depends on the resolution of the TF spectra, and SDTH, which depends on both the resolution of the TF spectra and the TF structure of the signals. These thresholds have both pros and cons: On one hand, the use of a specific threshold that takes into account the TF structure of the signals is appealing, but on the other, in a population study, its use implies an increase in the computational cost of the analysis. As shown in Fig. 3, only the SPWVD gives the possibility of using a signal-dependent threshold. This is an advantage over the MTSP. Nevertheless, the results of the simulation study (Fig. 7) show that the use of SDTH improved the accuracy of localization only for signals characterized by high SNR.

B. Comparison Between the Methodologies

Although the theoretical properties of an estimator of coherence based on SPWVD were first discussed in [16], [17], it was never used in biomedical applications. In the SPWVD, the reduction of the interference terms [19] is crucial since they may cause the coherence estimates to lose their physical meaning. In this study, the appropriate degree of smoothing was determined by first fixing a desired TF resolution, and then by iteratively increasing the degree of smoothing, until $\hat{\gamma}^{\mathrm{W}}(t, f) \in [0,\ 1]$. Another approach, presented in [28], makes use of geometrical relations between the TF structure of the signals and the interference terms to determine the parameter of the kernel (11). In that approach, as in [29], the support of the TFC is limited to regions of interest to reduce the required degree of smoothing.

By using both computer-generated and recorded physiological data, changes in the local coupling were better localized by SPWVD than MTSP. This is due to the same structural reason which makes the SPWVD more suitable than the spectrogram for the localization of TF features, namely, the possibility of independently setting the time and frequency filtering [18], [21]. Indeed, although the constraint of having a TFC bounded between 0 and 1 imposes a sort of tradeoff between time and frequency resolution, this option allows reducing the global amount of smoothing, thus yielding more accurate estimates. Nevertheless, the MTSP has some important features that could make it useful in coherence analysis. First, being based on spectrograms, which are non-negative, coherence estimates are always bounded between 0 and 1. Second, the use of Hermite functions, which are optimally concentrated in a circular TF region, offers a good tradeoff between time and frequency resolution [30], [31]. Finally, as shown in Fig. 6, it is also possible to detect local coupling between signals characterized by a low SNR via MTSP.

Both SPWVD and MTSP are characterized by a constant resolution over the entire TF domain. This is in contrast with other methodologies such as WT, in which the resolution depends on frequency. A uniform resolution makes the interpretation of the coherence function estimated by SPWVD and MTSP easier than the interpretation of the wavelet coherence since the uncertainty due to smoothing does not change with frequency. Moreover, as shown in Fig. 4, the SPWVD used in the simulation study was characterized by a finer resolution than the Morlet wavelets used previously in coherence analysis [10]. A comprehensive comparison between wavelet coherence and the methodologies presented in this study is beyond the scope of this paper. However, it is worth noting that although the resolution of the WT shown in Fig. 4 may be improved by choosing *ad hoc* parameters or other smoothing kernels [11], an improvement is likely to concern either time or frequency, since WT offers the same tradeoff between time and frequency as methods based on Fourier analysis [32].

Given that the main goal of time-frequency coherence analysis is to provide accurate estimates of local coupling, and given that the correct localization in both time and frequency accounts for most of the accuracy of the estimates, indices Δ^{m} and $\Delta^{(\mathrm{a}\%)}$ are used to quantify and compare the resolutions.

One of the differences between the SPWV-TFC and the TFC estimators based on spectrogram and continuous WT [10]–[12], [26], is that to estimate the SPWV-TFC, there is no need for further processing of the TF spectra. Indeed, by construction, the squared magnitude of the cross spectrogram (or scalogram) is equal to the product between the auto spectrograms (or scalograms). In single-trial coherence analysis, this implies that a further TF smoothing (a further decrease in TF resolution) than that used to estimate the spectra is required.

Spectrogram, wavelet, and SPWVD provide a spectral analysis that is formally equivalent [32], and they can be obtained by processing the Wigner–Ville distribution [18]. As previously mentioned, the advantage of SPWVD is that it offers the possibility of determining the shape of the smoothing function both in time and frequency, which, in turn, allows for more accurate localization of cardiovascular dynamics.

Recently, time-varying autoregressive methods were also proposed to estimate the coherence function [7], [8]. Time-frequency and autoregressive analysis are very different, and it is difficult to fairly compare them. However, TF analysis offers some advantages over autoregressive methods, which may deserve attention. In TF methods, the structure of the signals is characterized without imposing any assumption or model to the signals. No coefficient identification neither parameter initialization is needed. However, given that non-parametric TF methods do not rely on a model, they do not allow disentangling feedback and feedforward mechanisms when systems interact in closed-loop [7], [8].

C. Physiological Study

An analysis of the recorded physiological data showed that the methodologies described in this study can be used to characterize the dynamic interactions between cardiovascular signals. Generally, these signals have a nonstationary structure, even during intervals of supine position. This confirms that stationarity is an exception rather than the rule, and highlights the importance of TF analysis which, unless stationarity is proved [33], should be preferred to traditional time-invariant analysis. In this study, population-coherence analysis shows that during tilt table test, cardiovascular rhythms such as heart rate, systolic pressure, and respiratory signal, were dynamically coupled. Head-up tilt provoked an increase in the TFC between the RRV and SAPV signals. Moreover, it has been shown that the increase that followed the loss of coherence due to the postural changes (back and forth from supine position to head-up tilt), was characterized by similar slope. This may imply the presence of a common mechanism of resynchronization between RRV and SAPV. The presence of some artifacts due to the recalibration of the finger pressure signal may also be responsible for the decrease in the coupling observed at the beginning of T_{ht} and T_{ls}. The RRV and SAPV signals were also coupled in HF band, around respiratory rate. The strength of this coupling was similar to that between the RRV and RESP signals. This coupling, which is due to respiratory sinus arrhythmia, was maintained even during head-up tilt. Finally, it is shown that the PIV signal can be used as a surrogate for the RRV signal, even if caution is required in the HF band, where a decrease in the coherence during postural changes was observed. This may be due to a change in the vascular tone, which affects the pulse transit time and introduces a difference in the TF structure of the two signals [5].

Most of the algorithms described in this paper can be freely downloaded at http://www.micheleorini.com/.

REFERENCES

[1] G. C. Carter, "Coherence and time delay estimation," *Proc. IEEE*, vol. 75, no. 2, pp. 236–255, Feb. 1987.

[2] M. Di Rienzo, G. Parati, A. Radaelli, and P. Castiglioni, "Baroreflex contribution to blood pressure and heart rate oscillations: Time scales, time-variant characteristics and nonlinearities," *Phil. Trans. R. Soc. A*, vol. 367, no. 1892, pp. 1301–1318, Apr. 2009.

[3] M. Orini, L. T. Mainardi, E. Gil, P. Laguna, and R. Bailón, "Dynamic assessment of spontaneous baroreflex sensitivity by means of time-frequency analysis using either RR or pulse interval variability," in *Proc. 2010 Annu. Int. Conf. IEEE Eng. Med. Biol. Soc.*, pp. 1630–1633.

[4] K. Keissar, R. Maestri, G. D. Pinna, M. T. La Rovere, and O. Gilad, "Non-invasive baroreflex sensitivity assessment using wavelet transfer function-based time-frequency analysis," *Physiol. Meas.*, vol. 31, no. 7, pp. 1021–1036, Jul. 2010.

[5] E. Gil, M. Orini, R. Bailón, J. M. Vergara, L. T. Mainardi, and P. Laguna, "Photoplethysmography pulse rate variability as a surrogate measurement of heart rate variability during non-stationary conditions," *Physiol. Meas.*, vol. 31, no. 9, p. 1271, 2010.

[6] L. T. Mainardi, A. M. Bianchi, R. Furlan, S. Piazza, R. Barbieri, V. di Virgilio, A. Malliani, and S. Cerutti, "Multivariate time-variant identification of cardiovascular variability signals: A beat-to-beat spectral parameter estimation in vasovagal syncope," *IEEE Trans. Biomed. Eng.*, vol. 44, no. 10, pp. 978–989, Oct. 1997.

[7] H. Zhao, S. Lu, R. Zou, K. Ju, and K. H. Chon, "Estimation of time-varying coherence function using time-varying transfer functions," *Ann. Biomed. Eng.*, vol. 33, no. 11, pp. 1582–1594, Nov. 2005.

[8] H. Zhao, W. A. Cupples, K. H. Ju, and K. H. Chon, "Time-varying causal coherence function and its application to renal blood pressure and blood flow data," *IEEE Trans. Biomed. Eng.*, vol. 54, no. 12, pp. 2142–2150, Dec. 2007.

[9] S. Pola, A. Macerata, M. Emdin, and C. Marchesi, "Estimation of the power spectral density in nonstationary cardiovascular time series: Assessing the role of the time-frequency representations (TFR)," *IEEE Trans. Biomed. Eng.*, vol. 43, no. 1, p. 46, Jan. 1996.

[10] K. Keissar, L. R. Davrath, and S. Akselrod, "Coherence analysis between respiration and heart rate variability using continuous wavelet transform," *Phil. Trans. R. Soc. A*, vol. 367, no. 1892, pp. 1393–1406, 2009.

[11] J.-P. Lachaux, A. Lutz, D. Rudrauf, D. Cosmelli, M. L. V. Quyen, J. Martinerie, and F. Varela, "Estimating the time-course of coherence between single-trial brain signals: An introduction to wavelet coherence," *Neurophysiol. Clin.*, vol. 32, no. 3, pp. 157–174, Jun. 2002.

[12] Y. Zhan, D. Halliday, P. Jiang, X. Liu, and J. Feng, "Detecting time-dependent coherence between non-stationary electrophysiological signals—A combined statistical and time-frequency approach," *J. Neurosci. Methods*, vol. 156, no. 1–2, pp. 322–332, Sep. 2006.

[13] Y. Xu, S. Haykin, and R. J. Racine, "Multiple window time-frequency distribution and coherence of EEG using Slepian sequences and hermite functions," *IEEE Trans. Biomed. Eng.*, vol. 46, no. 7, pp. 861–866, Jul. 1999.

[14] E. G. Lovett and K. M. Ropella, "Time-frequency coherence analysis of atrial fibrillation termination during procainamide administration," *Ann. Biomed. Eng.*, vol. 25, no. 6, pp. 975–984, 1997.

[15] W. H. Cooke, J. B. Hoag, A. A. Crossman, T. A. Kuusela, K. U. O. Tahvanainen, and D. L. Eckberg, "Human responses to upright tilt: A window on central autonomic integration," *J. Physiol.*, vol. 517, no. 2, pp. 617–628, 1999.

[16] G. Matz and F. Hlawatsch, "Time-frequency coherence analysis of nonstationary random processes," in *Proc. IEEE Workshop Statist. Signal Array Process.*, 2000, pp. 554–558.

[17] L. B. White and B. Boashash, "Cross spectral analysis of nonstationary processes," *IEEE Trans. Inf. Theory*, vol. 36, no. 4, pp. 830–835, Jul. 1990.

[18] P. Flandrin, *Time-Frequency/Time-Scale Analysis*. New York: Academic, Ed., 1999.

[19] F. Hlawatsch and P. Flandrin, "The interference structure of the Wigner distribution and related time-frequency signal representations," in *The Wigner Distribution—Theory and Applications in Signal Processing*. Amsterdam, The Netherlands: Elsevier, 1997, pp. 59–113.

[20] A. Costa and G. Boudreau-Bartels, "Design of time-frequency representations using a multiform, tiltable exponential kernel," *IEEE Trans. Signal Process.*, vol. 43, no. 10, pp. 2283–2301, Oct. 1995.

[21] F. Hlawatsch and G. F. Boudreaux-Bartels, "Linear and quadratic time-frequency signal representations," *IEEE Signal Process. Mag.*, vol. 9, no. 2, pp. 21–67, Apr. 1992.

[22] D. Thomson, "Spectrum estimation and harmonic analysis," *Proc. IEEE*, vol. 70, no. 9, pp. 1055–1096, Sep. 1982.

[23] M. Bayram and R. Baraniuk, "Multiple window time-varying spectrum estimation," in *Nonlinear and Nonstationary Signal Processing*, William J. Fitzgerald, R. L. Smith, A. T. Walden, P. C. Young Eds. Cambridge, U.K.: Cambridge Univ. Press, 1996, pp. 292–316.

[24] J. Xiao and P. Flandrin, "Multitaper time-frequency reassignment for nonstationary spectrum estimation and chirp enhancement," *IEEE Trans. Signal Process.*, vol. 55, no. 6, pp. 2851–2860, Jun. 2007.

[25] A. Mincholé, E. Pueyo, J. F. Rodríguez, E. Zacur, M. Doblaré, and P. Laguna, "Quantification of restitution dispersion from the dynamic changes of the T-wave peak to end, measured at the surface ECG," *IEEE Trans. Biomed. Eng.*, vol. 58, no. 5, pp. 1172–1182, May 2011.

[26] A. Grinsted, J. C. Moore, and S. Jevrejeva, "Application of the cross wavelet transform and wavelet coherence to geophysical time series," *Nonlinear Process. Geophys.*, vol. 11, pp. 561–566, 2004.

[27] R. Bailón, P. Laguna, L. Mainardi, and L. Sornmo, "Analysis of heart rate variability using time-varying frequency bands based on respiratory frequency," in *Proc. Int. Conf. IEEE-EMBS*, Aug. 22–26, 2007, pp. 6674–6677.

[28] M. Orini, R. Bailón, L. Mainardi, A. Mincholé, and P. Laguna, "Continuous quantification of spectral coherence using quadratic time-frequency distributions: Error analysis and application," in *Proc. Comput. Cardiol.*, 2009, pp. 681–684.

[29] M. Muma, D. R. Iskander, and M. J. Collins, "The role of cardiopulmonary signals in the dynamics of the eye's wavefront aberrations," *IEEE Trans. Biomed. Eng.*, vol. 57, no. 2, pp. 373–383, Feb. 2010.

[30] P. Flandrin, "Maximum signal energy concentration in a time-frequency domain," in *Proc. Int Acoust., Speech, Signal Process. ICASSP-1988. Conf.*, pp. 2176–2179.

[31] I. Daubechies, "Time-frequency localization operators: A geometric phase space approach," *IEEE Trans. Inf. Theory*, vol. 34, no. 4, pp. 605–612, Jul. 1988.

[32] A. Bruns, "Fourier-, hilbert- and wavelet-based signal analysis: Are they really different approaches?" *J. Neurosci. Methods*, vol. 137, no. 2, pp. 321–332, Aug. 2004.

[33] P. Borgnat, P. Flandrin, P. Honeine, C. Richard, and J. Xiao, "Testing stationarity with surrogates: A time-frequency approach," *IEEE Trans. Signal Processing*, vol. 58, no. 7, pp. 3459–3470, Jul. 2010.

Authors' photographs and biographies not available at the time of publication.